

# A Simple Attempt for 3D Occupancy Estimation in Autonomous Driving

Wanshui Gan<sup>1,2</sup>

Ningkai Mo<sup>3</sup>

Hongbin Xu<sup>4</sup>

Naoto Yokoya<sup>1,2</sup>

<sup>1</sup>The University of Tokyo,<sup>2</sup>RIKEN

<sup>3</sup>Shenzhen Institute of Advanced Technology, Chinese Academy of Sciences

<sup>4</sup>South China University of Technology

{wanshuigan, nk.mo19941001, hongbinxu1013}@gmail.com, yokoya@k.u – tokyo.ac.jp

## Abstract

*The task of estimating 3D occupancy from surrounding-view images is an exciting development in the field of autonomous driving, following the success of Bird’s Eye View (BEV) perception. This task provides crucial 3D attributes of the driving environment, enhancing the overall understanding and perception of the surrounding space. However, there is still a lack of a baseline to define the task, such as network design, optimization, and evaluation. In this work, we present a simple attempt for 3D occupancy estimation, which is a CNN-based framework designed to reveal several key factors for 3D occupancy estimation. In addition, we explore the relationship between 3D occupancy estimation and other related tasks, such as monocular depth estimation, stereo matching, and BEV perception (3D object detection and map segmentation), which could advance the study on 3D occupancy estimation. For evaluation, we propose a simple sampling strategy to define the metric for occupancy evaluation, which is flexible for current public datasets. Moreover, we establish a new benchmark in terms of the depth estimation metric, where we compare our proposed method with monocular depth estimation methods on the DDAD and Nuscenes datasets. The relevant code will be available in <https://github.com/GANWANSHUI/SimpleOccupancy>.*

## 1. Introduction

3D scene understanding is a challenging mission for autonomous driving, especially only relying on the camera. In recent years, Bird’s Eye View (BEV) perception, including 3D detection [24] and map segmentation [21] is getting a lot of attention with the advantage of doing the 3D task estimation in the 2D feature plane and is beneficial for downstream tasks such as prediction and planning [26, 1]. However, some vital information for driving safety is ignored in

the BEV tasks, such as an unrecognizable obstacle. Therefore, reconstructing the 3D geometry of the driving scenes is a longstanding task for autonomous driving.

To obtain the 3D geometry information, depth estimation from RGB images, such as monocular depth estimation [8] and stereo matching [32], has been well investigated. While depth maps can provide 3D geometry information at the pixel level, we need to project them into the point cloud format in 3D space, and multiple post-processing procedures are required as depth maps may be inconsistent in the local region [10], which is not a straightforward manner for the 3D perception in autonomous driving. For better geometry representation in driving scenarios, occupancy estimation has gained attention in the industrial community. It has shown superiority over the representation in the BEV space [10]. However, for research purposes, there is still a lack of a baseline method for the public to measure the progress of occupancy estimation. Therefore, we explore a baseline for 3D occupancy estimation, starting from the surrounding-view setting, like BEV perception.

As an initial attempt in this field, we investigate the baseline in terms of network design, optimization, and evaluation. For the network design, as shown in Figure 1, the final output representation for 3D occupancy estimation is different from monocular depth estimation and stereo matching. The network architecture of the 3D occupancy estimation is similar to stereo matching, which means that the experiences from the stereo matching task can be adapted to occupancy estimation to reduce the burden in the network design. Therefore, we design the pipeline to resemble stereo matching closely and investigate a CNN-based framework as the baseline. In terms of optimization, we investigate two training fashions, including rendering-based [29] and classification-based loss functions. For evaluation, we conduct experiments on two well-known datasets, DDAD and Nuscenes [14, 3], for broader recognition. Besides, due to the lack of dense 3D occupancy labels for the two datasets,

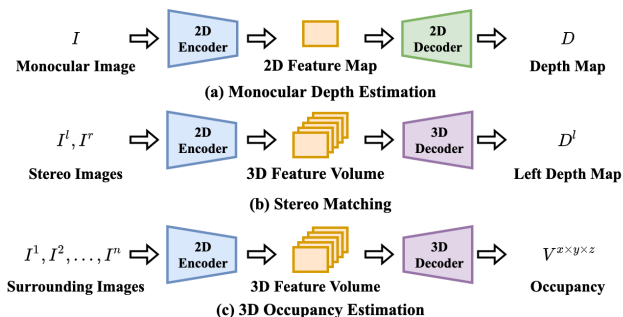


Figure 1. **The overall pipeline comparison of monocular depth estimation, stereo matching, and 3D occupancy estimation.**

we propose a novel distance-based metric for occupancy evaluation, which is inspired by the sampling strategy in volume rendering [29]. Our experimental results demonstrate that the proposed metric is more equitable compared to alternative options, such as classification metrics. Additionally, the proposed metric boasts flexibility as it solely relies on the point cloud as the ground truth, thereby eliminating any additional burdens when implementing the metric on similar datasets.

In summary, the main contributions of this work are as follows.

- Our study introduces a novel network design, loss design, and performance evaluation to investigate surrounding-view 3D occupancy estimation for the first time.
- To evaluate our proposed framework, we establish an occupancy metric for both the DDAD and Nuscenes datasets, and demonstrate the efficacy of the proposed metric for 3D occupancy evaluation. Furthermore, we connect 3D occupancy estimation to the monocular depth estimation task and establish a new ranking benchmark for DDAD and Nuscenes datasets based on the depth estimation metric.
- Through extensive qualitative and quantitative experiments, we demonstrate the effectiveness of our proposed method as a universal solution that can utilize existing datasets to do the 3D occupancy estimation and evaluation as simple as depth estimation.

## 2. Related Work

### 2.1. Depth estimation

For monocular depth estimation, it is usually implemented with a 2D U-Net architecture, as Figure 1 shown [13, 41]. More recently, the surrounding-view depth estimation has been explored, which is not just limited to a single image context [15, 39]. FSM [15] uses the spatio-temporal contexts, poses consistency constraints, and de-

signed photometric loss to learn a single network generating dense and scale-aware depth map. Differently, Surround-depth [39] adopts structure-from-motion to extract scale-aware pseudo depths to pretrain the models for the scale-aware result. This work mainly discusses 3D occupancy estimation, but we compare the depth metric with monocular depth estimation methods.

In terms of stereo matching, we could obtain the real scale depth map by estimating disparity between the stereo images. The state-of-the-art methods usually used 3D convolution neural networks (CNN) to do cost aggregation [7, 6, 40, 5, 11]. Likewise, we also used the 3D CNN to do 3D volume aggregation for the final occupancy representation.

### 2.2. BEV perception

We identify that the perception task from the bird’s eye view has a common step as the 3D occupancy estimation. Both of them require feature space transformation, where the BEV perception task is from the image space to the BEV plane [26], and 3D occupancy estimation is from the image space to the 3D volume space. LSS [31] implicitly projects the image feature to the 3d space by learning the latent depth distribution. DETR3D [38] and BEVFormer [23] define a 3D query in the 3D space and use the transformer attention mechanism to query the 2D image feature. ImVoxelNet [36] and Simple-BEV [16] build the 3D volume by the bilinear interpolation of the projection location at the 2D image feature plane, which is an efficient and parameter-free unprojection manner. Therefore, for simplicity in this baseline work, we adapt the parameter-free unprojection manner to build the 3D volume the same as Simple-BEV.

### 2.3. Occupancy estimation

There have been some works representing the scene in an occupancy (voxel) format [35, 28, 20]. Recently, the industrial community [10] reveals that the occupancy representation could be easily combined with the semantic information achieving instance-level prediction. Besides, it could predict the occupancy flow by considering the sequence frame, which could be regarded as the scene flow in the instance level [27]. Following [10], this personal blog gives a try to use volume rendering to train the occupancy representation in a self-supervision manner, which can not reconstruct the dynamic object and requires the velocity information of the vehicle [33]. For the geometry of driving scene, MonoScene [4] and Voxformer [22] explore the 3D semantic scene completion from a single image. This approach proposes to reconstruct the road scene from a monocular image by the deep implicit function [34]. Different from [4, 34, 22], we are under the surrounding-view setting, which is more challenging and meets the need for full perception in the driving scenarios. We need to

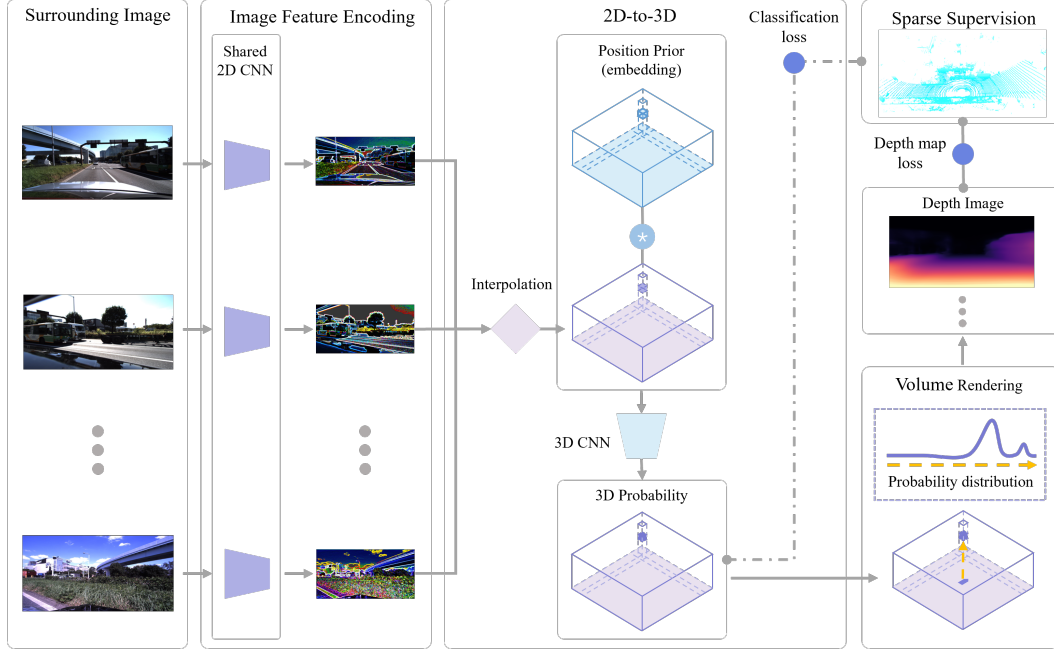


Figure 2. **The overview of the proposed Simple 3D Occupancy network (SimpleOccupancy).** Given the surrounding image, we first extract the image feature by the shared 2D CNN and then use the parameter-free interpolation to obtain the 3D volume. With the position prior guidance, the 3D CNN could effectively aggregate the 3D feature in the volume space (Section 3.2). At last, we train the proposed network by the depth map loss on the rendered depth map or the classification loss based on the occupancy label (Section 3.3 and 3.4).

point out that this baseline work is inspired by the above two works [10, 33] from industrial community, where we contribute a new CNN-based framework, a novel evaluation metric and set up the benchmark for both the 3D occupancy metric and depth map metric in the public datasets [14, 3].

At the time of writing this work, we found a preprint work TPVFormer [18], which is also for 3D occupancy estimation under the surrounding-view setting. Apart from the network architecture, the distinguishing difference is that we are investigating the pure geometry estimation (without considering the semantic information) from the novel optimization manner along with a novel evaluation metric. Our research investigates a more fundamental 3D perception task as close as depth estimation.

### 3. Method

#### 3.1. Preliminaries

In this paper, we adopt volume rendering to obtain the depth map for the model training. In the novel view synthesis task [29, 12], researchers usually use a multilayer perceptron network (MLP) to learn a mapping function to map the 3D position  $(x, y, z)$  and view direction  $(\theta, \phi)$  into the volume density  $\sigma$  and the RGB color  $c$ . For rendering the RGB value in a pixel, we can use the approximate volume rendering in NeRF [29] to do the weighted sum on the sampled point on the ray. The rendering function is defined in

the equation (1):

$$\hat{c} = \sum_{i=1}^W T_i (1 - \exp(-\sigma_i \delta_i) c_i), \quad (1)$$

where  $\hat{c}$  is the rendered RGB value,  $T_i = \exp(-\sum_{j=1}^{i-1} \sigma_j \delta_j)$ ,  $\delta_i = t_{i+1} - t_i$  is the adjacent sampled points' distance,  $i$  is the sampled point along the ray, and  $W$  is the number of the sampled points. If we want to obtain the depth information of the related pixel, we can replace the RGB value in the equation (1) with the sampled point's distance  $t_i$  as shown in equation (2). In this way, we can use the ground truth depth map to do the supervision training.

$$\hat{d} = \sum_{i=1}^W T_i (1 - \exp(-\sigma_i \delta_i) t_i). \quad (2)$$

The NeRF's model learns geometry by the multi-view constraint while, in our setting, the geometry is from the image that is achieved by the CNN model, as introduced below.

#### 3.2. Model design (SimpleOccupancy)

The problem setting of this work is defined in Figure 1. Given the surrounding-view images with the relative camera pose to the vehicle framework, we design an end-to-end neural network  $Q$  to predict the 3D occupancy map, where

we formulate it as  $Q: (I^1, I^2, I^3, \dots, I^n) \rightarrow V^{x \times y \times z}$ , where  $n$  is the number of the surrounding images and  $x, y, z$  represents the resolution of the final output of the voxel. We present the overview of the proposed framework in Figure 2, and give the details as follows.

**Encoder** For the image feature extraction, we use the ResNet [17] as the backbone. We provide the experiment on the ResNet 50 and 101 with the pre-trained model provided by Pytorch [30]. The final feature map is with the shape  $C \times H/4 \times W/4$ , where  $H$  and  $W$  are the input resolution of the image and  $C = 64$  is the channel number.

**From the image feature to 3D volume** For both the BEV perception and 3D occupancy estimation, a critical step is to transform the image feature from the 2D image space to the 3D volume space. In this baseline work, we adopt the simplest manner as used in the Simple-BEV [16]. The parameter-free transformation by the bilinear interpolation does not have any position prior, which means that the feature on the rays of the frustum is identical. Therefore, it is a highly ill-posed setting to infer the 3D geometry from the surrounding-view images with only a little overlap.

**3D volume space learning** The ill-posed setting requires stronger feature aggregation ability to achieve the 3D occupancy prediction. For the 3D feature learning, we adapt the 3D convolution network based on the hourglass structure from HybridNet [11] in the stereo-matching task. The transformer-based methods [22, 18, 10] use the position encoding to query the feature in the image space. Differently, after obtaining the 3D volume, we further learn position embedding to guide the 3D feature aggregation. The learned position embedding conducts the point-wise multiplication with the obtained 3D volume. The detailed network structure is placed in the supplementary material.

**Occupancy probability** After the 3D volume space feature aggregation, we have the final voxel  $V^{x \times y \times z}$ . The occupancy probability value is from the Sigmoid function (3).

$$Probability = Sigmoid(\sigma). \quad (3)$$

### 3.3. Model evaluation

To the best of our knowledge, we are the first work to explore the surrounding-view 3D occupancy estimation and the evaluation at the same time. Note that the concurrent work TPVFormer [18] did not investigate the evaluation in empty space. Therefore, we need to investigate the suitable metric to evaluate the model based on the available datasets, Nuscenes and DDAD datasets. We list the following key factors and facts that should be considered for the evaluation: (1) the current available outdoor dataset with the point cloud as the ground truth label is sparse, especially for the far-end space. Without huge efforts of human labeling, we can not obtain the dense voxel label as in [2]. Therefore, we can not evaluate the whole voxel space and could only

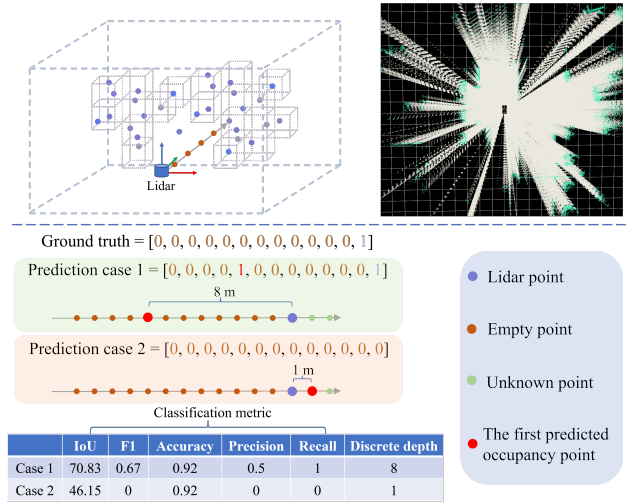


Figure 3. We use a collection of key points to represent the 3D space and evaluate it based on sample points. The classification label is shown on the upper side while the bottom side compares two metrics - the classification metric and our newly proposed discrete depth metric - in two different prediction cases. It is evident that the discrete depth metric accurately reflects the cost associated with each prediction.

do the evaluation on the known space. (2) About the known space, we can only determine the space between the lidar center and the point cloud. (3) The 3D occupancy and voxel representation is a discrete representation, which means the quantization error is unavoidable, but we can determine the affordable quantization error in the autonomous driving scenario. (4) The evaluation should be feasible for the common datasets and easily be conducted for the study. Our goal with this work is to explore a pipeline that can leverage existing datasets used for depth estimation to perform 3D occupancy estimation and evaluation. Therefore, given the aforementioned considerations, we examine two evaluation metrics in this study: the classification metric and the discrete depth metric. These metrics are also associated with two training fashions in the ablation study as shown in Figure 3.

**Occupancy label generation** Inspired by NeRF [29], we use the stratified sampling strategy to set the label for the free space. First, we set Lidar’s position as the origin of all the rays for all the point clouds. Different from the even stride sampling, we use a fixed number of sample points (30), which means that, for closer point clouds, the sampling space is denser, and for far-end point clouds, the sampling space is sparser. The used sampling strategy has advantages in that it allows for a more balanced distribution of positive and negative labels and maintains a higher standard for closer objects in the driving scenes. The occupied space is represented by the down-sampled point cloud, where we

set the down-sample size as 0.4 m. The above operation can be easily performed using the Open3D [42] library.

**Classification metric** By representing the known space by a set of key points, we can perform the evaluation as the classification task with binary classification metrics, as shown in Figure 3. The classification metrics are commonly used in 3D semantic scene completion tasks [35, 4, 22]. However, we observe that classification metrics are not perfect since they can only evaluate the known space in our setting. We give two cases of evaluation along a ray in Figure 3. We can see that classification metric is not sensitive to case 1. Even though the first predicted occupancy point is far away from the ground truth occupancy (lidar point), classification metric still gives a high score. Conversely, in case 2, if the network is unable to predict the first occupancy point in known space, all of the classification metrics produce a low score except for the accuracy metric. This is unfair if the first predicted occupancy point is next to the actual occupancy point. For a more detailed explanation, please refer to the supplementary material.

**Discrete depth metric** Recognizing the limitations of classification metric, we introduce discrete depth metric, which provides a more accurate assessment of predictions. Our approach involves dense sampling evaluation points along the ray with an interval (0.2 m) and a maximum distance (52 m). If all the prediction along the ray is empty, we set the last point as the first predicted occupancy point. The discrete depth error is then calculated as the distance between the first predicted occupancy point and point cloud along the ray. By utilizing this criterion, we can perform evaluations in a manner similar to depth map error assessments. Following depth estimation [39], we report occupancy evaluation with the following metrics, including error metric, (Abs Rel, Sq Rel, RMSE, RMSE log) and accuracy metric,  $\delta < t : \% \text{ of } d \text{ s.t. } \max\left(\frac{\hat{d}}{d^*}, \frac{d^*}{\hat{d}}\right) = \delta < t$ . The detailed definition is presented in supplementary material.

### 3.4. Model optimization

Based on the available depth map and the generated occupancy label as introduced before, we investigate two different training manners. The first one is depth loss, the depth map supervision by the volume rendering. The other one directly calculates the binary classification loss based on the obtained label in the known space, where we consider binary cross entropy loss and L1 loss.

**Depth loss** With the depth map from the volume rendering, we can train the network the same as the depth estimation task. Following [41], we use the Scale-Invariant Logarithmic (SILog) loss [9] to supervise the training. Specifi-

cally, the depth map loss is defined as:

$$\mathcal{L}_{depth} = \alpha \sqrt{\frac{1}{M} \sum_i \Delta d_i^2 - \frac{\lambda}{M^2} \left( \sum_i \Delta d_i \right)^2}, \quad (4)$$

where  $\Delta d_i = \log \hat{d}_i - \log d_i^*$ ,  $d_i^*$  is the ground truth depth and  $\hat{d}_i$  is the predicted depth.  $M$  is the number of valid pixels. We set  $\lambda = 0.85$  and  $\alpha = 10$  the same as [41].

**Classification loss** Following the common practice, we use the binary cross entropy loss function to train the model as follows:

$$\mathcal{L}_{BCE} = -\frac{1}{N} \sum_{i=1}^N y_i \cdot \log(\hat{y}_i) + (1 - y_i) \cdot \log(1 - \hat{y}_i), \quad (5)$$

where  $y_i$  is the ground truth label and  $\hat{y}_i$  is the prediction. Besides, we also investigate to use of the L1 loss direct work on sampled points as below:

$$\mathcal{L}_{L1} = \frac{1}{N} \sum_{i=1}^N L_1(1 - p_i) + \frac{1}{K} \omega \sum_{j=1}^K L_1(0 - p_j), \quad (6)$$

where  $p_i$  is the probability value based on the point cloud position, and  $p_j$  is the probability value from the sampled point in the empty space.  $N$  is the number of the valid point cloud and  $K$  is the number of sampled points in the empty space.  $\omega = 5$  is the hyperparameter for balancing occupied and empty labels with the search range from 1 to 10.0.

## 4. Experiment

Currently, there is a lack of established baseline work for surrounding-view 3D occupancy estimation. Therefore, we present the first attempt at addressing this gap by evaluating our proposed framework on DDAD and Nuscenes datasets. Our experiments consist of two parts. First, we conduct a detailed ablation study on the proposed framework to investigate the characteristics of the loss function and network design. Second, as we can obtain the depth map through volume rendering, we establish a benchmark for depth metrics by comparing our results with those of monocular depth estimation methods under the supervision setting.

### 4.1. Datasets

**DDAD** [14] is a largescale dataset with dense ground-truth depth maps. Specifically, this dataset includes 12,650 training samples. The validation set contains 3,950 samples. We only consider the distance up to 52m, which is a reasonable range referred from the 3D semantic completion task [4] and BEV perception task [23]. The DDAD dataset has a denser point cloud compared with Nuscenes dataset, which could provide a more equitable evaluation, so we conduct an ablation study experiment based on the DDAD dataset.

DDAD [14]													
Experiment setting						Discrete depth metric							
	$\mathcal{L}_{depth}$	$\mathcal{L}_{BCE}$	$\mathcal{L}_{L1}$	Prior	Res101	LSS [31]	Abs Rel ↓	Sq Rel ↓	RMSE ↓	RMSE log ↓	$\delta < 1.25 \uparrow$	$\delta < 1.25^2 \uparrow$	$\delta < 1.25^3 \uparrow$
(1)	✓						0.210	2.724	9.595	0.343	0.674	0.869	0.936
(2)		✓					0.235	3.395	10.692	0.418	0.647	0.837	0.908
(3)			✓				0.231	3.916	12.365	0.413	0.650	0.834	0.905
(4)	✓			✓			<b>0.206</b>	<b>2.644</b>	<u>9.457</u>	<u>0.342</u>	<u>0.686</u>	<u>0.875</u>	<u>0.937</u>
(5)	✓			✓	✓		<b>0.206</b>	2.655	<b>9.422</b>	<b>0.339</b>	<b>0.690</b>	<b>0.877</b>	<b>0.939</b>
(6)	✓			✓	✓*		0.264	3.940	10.512	0.378	0.617	0.836	0.918
(7)	✓			✓	✓	✓	<u>0.207</u>	<u>2.651</u>	9.684	0.348	0.668	0.863	0.930
Nuscenes [3]													
(5)	✓			✓	✓		0.537	13.710	13.666	0.541	0.485	0.719	0.850

Table 1. The ablation study of the proposed method in the proposed discrete depth metric for occupancy evaluation. Experiment (6) means do not use the official pretrained model for ResNet 101. Experiment (5) is the full model.  $\uparrow$  means the value higher is better and  $\downarrow$  means lower is better. The number with bold typeface means the best and the number with the underline is the second.

DDAD [14]			
Experiment setting	Depth metric		
	Abs Rel ↓	Sq Rel ↓	$\delta < 1.25 \uparrow$
(1)	0.152	1.034	0.795
(2)	0.239	3.358	0.744
(3)	0.176	1.699	0.710
(4)	<u>0.150</u>	<u>1.019</u>	<u>0.798</u>
(5)	<b>0.148</b>	<b>1.000</b>	<b>0.800</b>
(6)	0.204	1.663	0.702
(7)	<b>0.148</b>	1.029	<u>0.798</u>
Nuscenes [3]			
(5)	0.118	0.579	0.891

Table 2. The ablation study of the proposed method in the depth metric. The full table is presented in the supplementary material.

**Nuscenes** [3] has 1000 sequences of diverse scenes, where each sequence is approximately 20 seconds in duration. We split the training and testing set the same as the depth estimation task [39], including 20096 samples for training and 6019 samples for validation. The distance is also limited to 52m for consideration.

For the above two datasets, we generate the occupancy and empty space label from the raw point cloud and use the projected depth map for training and testing. Specifically, we first define the  $Z$ ,  $Y$ , and  $X$  as depth, height, and width, respectively. For the similar perception range as SemanticKITTI [2], the valid point cloud range is set as  $Z \in (-52m, 52m)$ ,  $Y \in (0m, 6m)$ , and  $X \in (-52m, 52m)$  for the training and testing. With the final voxel resolution in  $256 \times 256 \times 16$ , the size of the resolutions of the grid is (0.41m, 0.41m, 0.38m). At last, we set the best threshold for obtaining the score of discrete depth metric from the search range from 0 to 1 with an interval of 0.05.

## 4.2. Implementation detail

Our approach is implemented with Pytorch [30]. We resize the RGB image into  $336 \times 672$  before putting them into the neural network. The depth map is rendered with the resolution  $224 \times 352$ . We use the Adam optimizer [19] with

$\beta_1 = 0.9$  and  $\beta_2 = 0.999$ . The learning rate of the 2D CNN is set as  $1e - 4$  and the 3D CNN is  $1e - 3$ . We train the networks with 12 epochs and do the learning rate decay with 0.1 at the 10th epoch. All the experiments have been conducted on the NVIDIA A 100 (40 GB) GPU.

## 4.3. The ablation study for the proposed framework

We present the ablation study result of the proposed method in Table 1 (discrete depth metric) and Table 2 (depth metric). We mainly investigate the characteristics of the different loss functions and the network design as follows:

**Loss functions analysis** First, we conduct the experiment with different loss functions based on the baseline model. We can see that the depth loss outperforms the classification for both the discrete depth metric and the depth metric in Table 1 and Table 2. Accompanying with Figure 4 marked with white circles in the depth map and the dense occupancy map, we can observe that the classification losses easily produce the floater, especially in the region close to the sky, because the training could not handle these regions behind the point cloud. Reversely, the depth loss could largely prevent this situation because the rendering fashion cloud implicitly optimizes these regions with the sampled points along the whole ray. But there is still some extreme section, such as at the top of the ego vehicle, exists the floater problem, which never has the sample point to optimize that region. On the other hand, we could observe that the classification loss could produce sharper occupancy boundaries, and the depth loss from rendering more easily produced the long tail false positive prediction as marked with the green circles. The long tail false positive prediction usually happens at the intersection of the foreground and the background, which also happens in the stereo matching task [37]. For pixel-level (ray level) prediction, depth supervision with volume rendering is similar to the disparity estimation by the softmax operation. The solution in [37] may help to address the long tail false positive prediction problem, which deserves to investigate in the

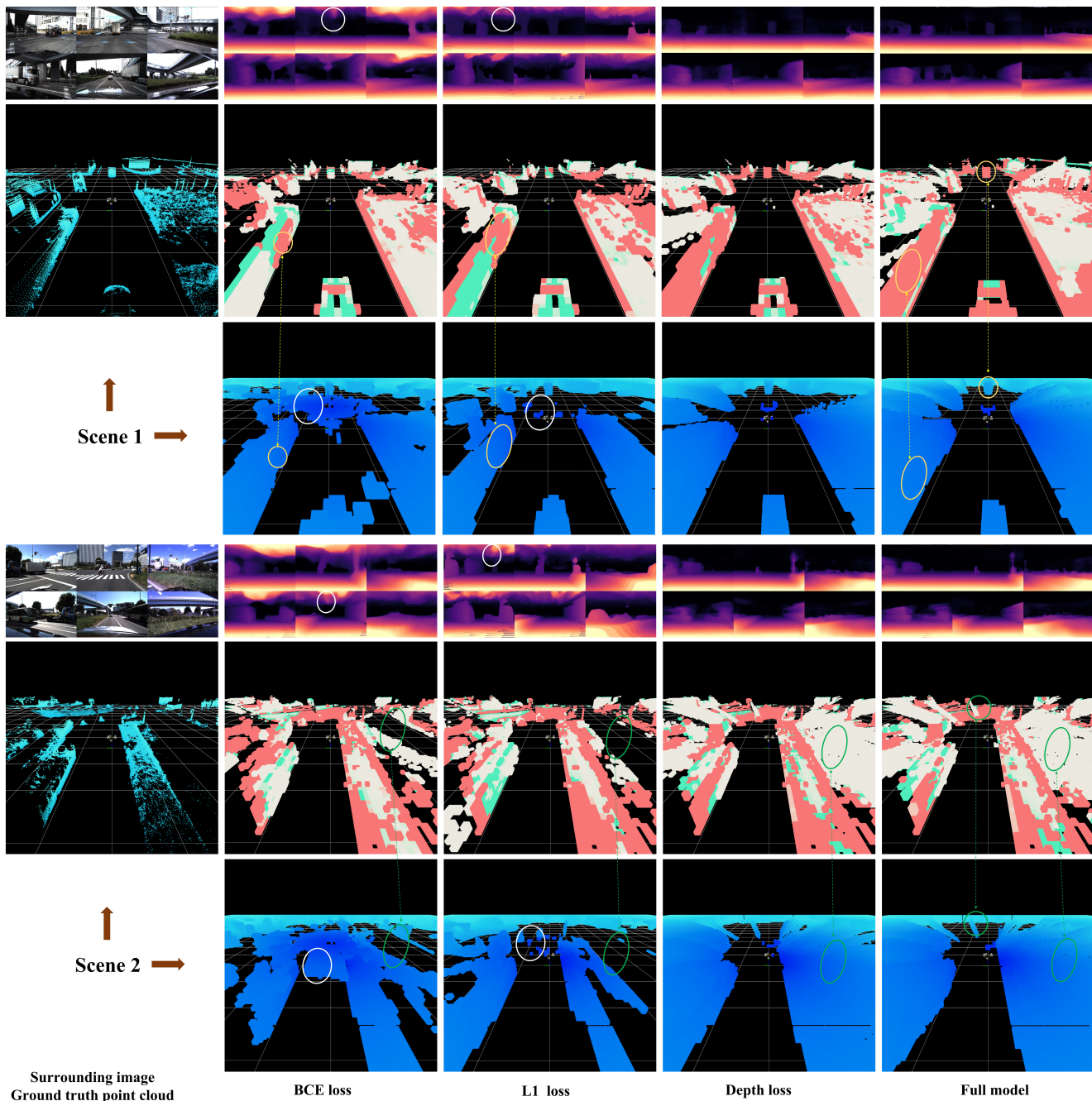


Figure 4. **The visualization for the ablation study of the proposed method (DDAD dataset [14]).** The first row: the surrounding images and the rendered depth maps. For the second row: based on the occupancy label, we present the binary prediction, where the red, green, and white colors mean the false negative, true positive, and false positive, respectively. The third row is the dense occupancy prediction in the voxel grid, where the darker color means the occupancy is closer to the ego vehicle. The BCE loss, L1 loss, Depth loss, and Full model are related to the experiment setting (2), (3), (1), and (5) in Table 1 and 2, respectively. Note that we omit the prediction under the 0.4 m for better visualization. Best viewed in color.

future.

In terms of the metric design, the prediction case 2 in Figure 3 usually happens as marked with yellow circles, where the network fails to predict the first occupancy at the

end of the point cloud, but in the real situation, the first occupied point is very close to the point cloud from the visualization of the dense occupancy. Therefore, the proposed discrete depth metric could have a more justice assessment

Method	Occupancy	Depth	Abs Rel	Sq Rel	RMSE	RMSE log	$\delta < 1.25$	$\delta < 1.25^2$	$\delta < 1.25^3$	Inference time (s)
DDAD [14]										
Monodepth2 [13]	✗	✓	0.148	1.003	4.722	0.219	0.795	0.935	0.973	<b>0.029</b>
New-CRFs [41]	✗	✓	<b>0.130</b>	<b>0.824</b>	<b>4.169</b>	<b>0.195</b>	<b>0.840</b>	<b>0.951</b>	<b>0.979</b>	0.065
Surrounddepth [39]	✗	✓	0.151	1.021	4.766	0.221	0.789	0.935	0.974	0.099
Ours	✓	✓	0.148	1.00	4.770	0.220	0.800	0.935	0.973	0.230
Nuscenes [3]										
Monodepth2 [13]	✗	✓	0.131	0.728	3.479	0.201	0.845	0.942	0.974	<b>0.024</b>
New-CRFs [41]	✗	✓	<b>0.115</b>	0.618	3.193	0.185	0.872	0.951	<b>0.977</b>	0.058
Surrounddepth [39]	✗	✓	0.128	0.760	3.442	0.198	0.856	0.946	0.975	0.102
Ours	✓	✓	0.118	<b>0.579</b>	<b>2.63</b>	<b>0.178</b>	<b>0.891</b>	<b>0.954</b>	<b>0.977</b>	0.196

Table 3. The benchmark in depth map metric with monocular depth estimation methods. The number with bold typeface means the best.

for the 3D occupancy estimation.

**Network design** Based on the depth loss, we further investigate the network design. To alleviate the highly ill-posed problem setting, we learn position embedding to guide the 3D feature aggregation. From Table 1 and Table 2, we can see that experiment (4) with position prior achieves better results. Furthermore, by replacing ResNet 50 with ResNet 101, the model gets another performance gain. Note that, in experiment (6), the model got a severe performance drop without initializing the pretrain model from Pytorch, which hints that finding a better pretrain strategy associated with 3D occupancy estimation may further boost the performance. The used parameter-free interpolation to recover 3D feature space is the most straightforward and efficient manner. In addition, we also try to use the unprojection manner proposed in LSS [31], which estimates the depth distribution first, and then forms the 3D volume with the weighted feature based on the distribution information. However, we overlooked the benefit of LSS’s unprojection manner on the 3D occupancy estimation task, which gives us the information that doing the depth distribution estimation may cause a larger learning space for the following 3D CNN feature aggregation module, especially under the imperfect depth distribution estimation.

**Nuscenes** We also implement the experiment setting (5) to the Nuscenes dataset. The visualization result and analysis are placed in the supplement due to limited space.

In a brief summary, from Table 1 and Table 2, we can conclude that the proposed discrete depth metric for 3D occupancy evaluation is related to the depth metric. In general, with better depth map results and the 3D occupancy prediction is also better. From Figure 4, we can see that the model could predict the reasonable layout of the driving scenes, but some details are still missing, and the far-end prediction is still not good. We discuss the improvement in the future work section.

#### 4.4. The benchmark for the depth estimation

In the surrounding-view setting, we build a new benchmark in terms of the depth map metric for comparison with

the monocular depth estimation methods. Monodepth2 [13] is a well-recognized self-supervision monocular depth estimation method and New-CRFs [41] is the state-of-the-art supervision method. Surrounddepth [39] is a self-supervision work that has been introduced in the related work. For the supervision setting in this work, we train the above three monocular depth estimation methods with the same loss function used in [41].

From Table 3, we can observe that our method is competitive with the monocular depth estimation methods. For the DDAD dataset, New-CRFs [41] achieves the best result, matching its performance in single image depth estimation. The performance for Monodepth2 [13], Surrounddepth [39], and ours is similar. For the Nuscenes dataset, our method achieves the best result. The visualization result is presented in the supplementary material.

The disadvantage of our method is that the inference time is higher than the monocular depth estimation methods. We further analyze the inference time for each component of the system. For the DDAD dataset: 2D CNN (31) + 2D to 3D interpolation (3) + 3D CNN (101) + Rendering (95) = 230 (ms). We learn that the 3D feature aggregation and the rendering of the depth map occupied the main time. Note that Rendering is for depth maps and is ignorable if we only want the occupancy estimation.

## 5. Limitation and future work

In this simple attempt for 3D occupancy estimation, we still do not introduce the sequence information as did in [10] and the BEV perception tasks [23, 25]. It is a promising direction to improve performance by fusing the sequence information. Besides, the current voxel resolution is relatively coarse with 0.4 m, which is a good beginning for the research purpose due to limited computational resources. In the future, we will explore a higher resolution such as 0.2 m [4]. Besides, as observed in Figure 4, the classification loss generally produces sharper boundary than depth loss but with the floater problem, we would investigate the combination of these two training manners to see the benefit.



## 6. Conclusion

In this paper, we established a baseline for 3D occupancy estimation in the surrounding-view setting for autonomous driving. We demonstrated the effectiveness of the entire pipeline through novel network design, loss function investigation, and model evaluation. We hope this baseline work will inspire followers, and we will release the code to encourage further research in this field.

## References

- [1] Eduardo Arnold, Omar Y Al-Jarrah, Mehrdad Dianati, Saber Fallah, David Oxtoby, and Alex Mouzakitis. A survey on 3d object detection methods for autonomous driving applications. *IEEE Transactions on Intelligent Transportation Systems*, 20(10):3782–3795, 2019. 1
- [2] Jens Behley, Martin Garbade, Andres Milioto, Jan Quenzel, Sven Behnke, Cyrill Stachniss, and Jurgen Gall. Semantickitti: A dataset for semantic scene understanding of lidar sequences. In *Proceedings of the IEEE/CVF International Conference on Computer Vision*, pages 9297–9307, 2019. 4, 6
- [3] Holger Caesar, Varun Bankiti, Alex H Lang, Sourabh Vora, Venice Erin Liong, Qiang Xu, Anush Krishnan, Yu Pan, Giancarlo Baldan, and Oscar Beijbom. nuscenes: A multi-modal dataset for autonomous driving. In *Proceedings of the IEEE/CVF conference on computer vision and pattern recognition*, pages 11621–11631, 2020. 1, 3, 6, 8
- [4] Anh-Quan Cao and Raoul de Charette. Monoscene: Monocular 3d semantic scene completion. In *Proceedings of the IEEE/CVF Conference on Computer Vision and Pattern Recognition*, pages 3991–4001, 2022. 2, 5, 8
- [5] Jia-Ren Chang and Yong-Sheng Chen. Pyramid stereo matching network. In *Proceedings of the IEEE conference on computer vision and pattern recognition*, pages 5410–5418, 2018. 2
- [6] Xinjing Cheng, Peng Wang, and Ruigang Yang. Learning depth with convolutional spatial propagation network. *IEEE transactions on pattern analysis and machine intelligence*, 42(10):2361–2379, 2019. 2
- [7] Xuelian Cheng, Yiran Zhong, Mehrtash Harandi, Yuchao Dai, Xiaojun Chang, Hongdong Li, Tom Drummond, and Zongyuan Ge. Hierarchical neural architecture search for deep stereo matching. *Advances in Neural Information Processing Systems*, 33:22158–22169, 2020. 2
- [8] Xingshuai Dong, Matthew A Garratt, Sreenatha G Anavatti, and Hussein A Abbass. Towards real-time monocular depth estimation for robotics: A survey [-5pt]. *IEEE Transactions on Intelligent Transportation Systems*, 2022. 1
- [9] David Eigen, Christian Puhrsch, and Rob Fergus. Depth map prediction from a single image using a multi-scale deep network. *Advances in neural information processing systems*, 27, 2014. 5
- [10] Ashok Elluswamy. Occupancy network. [https://www.youtube.com/watch?v=ODSJsviD\\_SU&t=4331s](https://www.youtube.com/watch?v=ODSJsviD_SU&t=4331s). Accessed Mar. 08, 2023 [Online]. 1, 2, 3, 4, 8
- [11] Wanshui Gan, Wenhao Wu, Shifeng Chen, Yuxiang Zhao, and Pak Kin Wong. Rethinking 3d cost aggregation in stereo matching. *Pattern Recognition Letters*, 2023. 2, 4
- [12] Wanshui Gan, Hongbin Xu, Yi Huang, Shifeng Chen, and Naoto Yokoya. V4d: Voxel for 4d novel view synthesis. *arXiv preprint arXiv:2205.14332*, 2022. 3
- [13] Clément Godard, Oisín Mac Aodha, Michael Firman, and Gabriel J Brostow. Digging into self-supervised monocular depth estimation. In *Proceedings of the IEEE/CVF International Conference on Computer Vision*, pages 3828–3838, 2019. 2, 8
- [14] Vitor Guizilini, Rares Ambrus, Sudeep Pillai, Allan Raveentos, and Adrien Gaidon. 3d packing for self-supervised monocular depth estimation. In *Proceedings of the IEEE/CVF Conference on Computer Vision and Pattern Recognition*, pages 2485–2494, 2020. 1, 3, 5, 6, 7, 8
- [15] Vitor Guizilini, Igor Vasiljevic, Rares Ambrus, Greg Shakhnarovich, and Adrien Gaidon. Full surround monodepth from multiple cameras. *IEEE Robotics and Automation Letters*, 7(2):5397–5404, 2022. 2
- [16] Adam W Harley, Zhaoyuan Fang, Jie Li, Rares Ambrus, and Katerina Fragkiadaki. Simple-bev: What really matters for multi-sensor bev perception? *arXiv preprint arXiv:2206.07959*, 2022. 2, 4
- [17] Kaiming He, Xiangyu Zhang, Shaoqing Ren, and Jian Sun. Deep residual learning for image recognition. In *Proceedings of the IEEE conference on computer vision and pattern recognition*, pages 770–778, 2016. 4
- [18] Yuanhui Huang, Wenzhao Zheng, Yunpeng Zhang, Jie Zhou, and Jiwen Lu. Tri-perspective view for vision-based 3d semantic occupancy prediction. *arXiv preprint arXiv:2302.07817*, 2023. 3, 4
- [19] Diederik P Kingma and Jimmy Ba. Adam: A method for stochastic optimization. *arXiv preprint arXiv:1412.6980*, 2014. 6
- [20] Bernard Lange, Masha Itkina, and Mykel J Kochenderfer. Lopr: Latent occupancy prediction using generative models. *arXiv preprint arXiv:2210.01249*, 2022. 2
- [21] Qi Li, Yue Wang, Yilun Wang, and Hang Zhao. Hdmapiet: An online hd map construction and evaluation framework. In *2022 International Conference on Robotics and Automation (ICRA)*, pages 4628–4634. IEEE, 2022. 1
- [22] Yiming Li, Zhiding Yu, Christopher Choy, Chaowei Xiao, Jose M Alvarez, Sanja Fidler, Chen Feng, and Anima Anandkumar. Voxformer: Sparse voxel transformer for camera-based 3d semantic scene completion. *arXiv preprint arXiv:2302.12251*, 2023. 2, 4, 5
- [23] Zhiqi Li, Wenhao Wang, Hongyang Li, Enze Xie, Chonghao Sima, Tong Lu, Qiao Yu, and Jifeng Dai. Bevformer: Learning bird’s-eye-view representation from multi-camera images via spatiotemporal transformers. *arXiv preprint arXiv:2203.17270*, 2022. 2, 5, 8
- [24] Yingfei Liu, Tiancai Wang, Xiangyu Zhang, and Jian Sun. Petr: Position embedding transformation for multi-view 3d object detection. *arXiv preprint arXiv:2203.05625*, 2022. 1
- [25] Yingfei Liu, Junjie Yan, Fan Jia, Shuailin Li, Qi Gao, Tiancai Wang, Xiangyu Zhang, and Jian Sun. Petr2: A uni-

- fied framework for 3d perception from multi-camera images. *arXiv preprint arXiv:2206.01256*, 2022. 8
- [26] Yuexin Ma, Tai Wang, Xuyang Bai, Huitong Yang, Yuenan Hou, Yaming Wang, Yu Qiao, Ruigang Yang, Dinesh Manocha, and Xinge Zhu. Vision-centric bev perception: A survey. *arXiv preprint arXiv:2208.02797*, 2022. 1, 2
- [27] Moritz Menze and Andreas Geiger. Object scene flow for autonomous vehicles. In *Proceedings of the IEEE conference on computer vision and pattern recognition*, pages 3061–3070, 2015. 2
- [28] Lars Mescheder, Michael Oechsle, Michael Niemeyer, Sebastian Nowozin, and Andreas Geiger. Occupancy networks: Learning 3d reconstruction in function space. In *Proceedings of the IEEE/CVF conference on computer vision and pattern recognition*, pages 4460–4470, 2019. 2
- [29] Ben Mildenhall, Pratul P Srinivasan, Matthew Tancik, Jonathan T Barron, Ravi Ramamoorthi, and Ren Ng. Nerf: Representing scenes as neural radiance fields for view synthesis. *Communications of the ACM*, 65(1):99–106, 2021. 1, 2, 3, 4
- [30] Adam Paszke, Sam Gross, Soumith Chintala, Gregory Chanan, Edward Yang, Zachary DeVito, Zeming Lin, Alban Desmaison, Luca Antiga, and Adam Lerer. Automatic differentiation in pytorch. 2017. 4, 6
- [31] Jonah Philion and Sanja Fidler. Lift, splat, shoot: Encoding images from arbitrary camera rigs by implicitly unprojecting to 3d. In *European Conference on Computer Vision*, pages 194–210. Springer, 2020. 2, 6, 8
- [32] Matteo Poggi, Fabio Tosi, Konstantinos Batsos, Philippos Mordohai, and Stefano Mattoccia. On the synergies between machine learning and binocular stereo for depth estimation from images: a survey. *IEEE Transactions on Pattern Analysis and Machine Intelligence*, 44(9):5314–5334, 2021. 1
- [33] Tristan Rice. Voxnet. <https://fn.lc/post/voxel-sfm/>. Accessed Mar. 08, 2023 [Online]. 2, 3
- [34] Thomas Roddick, Benjamin Biggs, Daniel Olmeda Reino, and Roberto Cipolla. On the road to large-scale 3d monocular scene reconstruction using deep implicit functions. In *Proceedings of the IEEE/CVF International Conference on Computer Vision*, pages 2875–2884, 2021. 2
- [35] Luis Roldao, Raoul De Charette, and Anne Verroust-Blondet. 3d semantic scene completion: a survey. *International Journal of Computer Vision*, pages 1–28, 2022. 2, 5
- [36] Danila Rukhovich, Anna Vorontsova, and Anton Konushin. Imvoxnet: Image to voxels projection for monocular and multi-view general-purpose 3d object detection. In *Proceedings of the IEEE/CVF Winter Conference on Applications of Computer Vision*, pages 2397–2406, 2022. 2
- [37] Fabio Tosi, Yiyi Liao, Carolin Schmitt, and Andreas Geiger. Smd-nets: Stereo mixture density networks. In *Proceedings of the IEEE/CVF Conference on Computer Vision and Pattern Recognition*, pages 8942–8952, 2021. 6
- [38] Yue Wang, Vitor Campagnolo Guizilini, Tianyuan Zhang, Yilun Wang, Hang Zhao, and Justin Solomon. Detr3d: 3d object detection from multi-view images via 3d-to-2d queries. In *Conference on Robot Learning*, pages 180–191. PMLR, 2022. 2
- [39] Yi Wei, Linqing Zhao, Wenzhao Zheng, Zheng Zhu, Yongming Rao, Guan Huang, Jiwen Lu, and Jie Zhou. Surrounddepth: Entangling surrounding views for self-supervised multi-camera depth estimation. *arXiv preprint arXiv:2204.03636*, 2022. 2, 5, 6, 8
- [40] Gangwei Xu, Junda Cheng, Peng Guo, and Xin Yang. Attention concatenation volume for accurate and efficient stereo matching. In *Proceedings of the IEEE/CVF Conference on Computer Vision and Pattern Recognition*, pages 12981–12990, 2022. 2
- [41] Weihao Yuan, Xiaodong Gu, Zuozhuo Dai, Siyu Zhu, and Ping Tan. Newcrfs: Neural window fully-connected crfs for monocular depth estimation. In *Proceedings of the IEEE Conference on Computer Vision and Pattern Recognition*, 2022. 2, 5, 8
- [42] Qian-Yi Zhou, Jaesik Park, and Vladlen Koltun. Open3d: A modern library for 3d data processing. *arXiv preprint arXiv:1801.09847*, 2018. 5